Thin Solid Films 628 (2017) 1–6

Contents lists available at ScienceDirect

Thin Solid Films

journal homepage: www.elsevier.com/locate/tsf

Cu_2ZnSnS_4-based thin films and solar cells by rapid thermal annealing processing

M.A. Olgar [a,b,*], J. Klaer [a], R. Mainz [a], L. Ozyuzer [c], T. Unold [a]

[a] Helmholtz Zentrum Berlin Mat & Energie GmbH, D-14109 Berlin, Germany
[b] Department of Physics, Karadeniz Technical University, 61080 Trabzon, Turkey
[c] Department of Physics, Izmir Institute of Technology, Urla, Izmir, Turkey

ARTICLE INFO

Article history:
Received 18 June 2016
Received in revised form 21 February 2017
Accepted 3 March 2017
Available online 6 March 2017

Keywords:
Thin film solar cells
Cu_2ZnSnS_4 (CZTS)
Sputtering
RTP
Pre-annealing
Kesterite

ABSTRACT

In this study, kesterite Cu_2ZnSnS_4 (CZTS) absorber layers were fabricated by DC magnetron sputtering deposition of metallic Cu-Zn-Sn precursors, followed by an annealing treatment in sulfur vapor atmosphere at 600 °C for 3 min using rapid thermal processing (RTP). Three types of stacked metallic films were prepared and included pre-annealing of Cu-Sn stacks in order to induce preferential Cu-Sn alloying. The chemical composition of the sulfurized films was obtained by X-ray fluorescence (XRF) before and after etching the samples in KCN solution. All CZTS thin films are found to be Cu-poor and Zn-rich. Structural characterizations were performed by X-ray diffraction (XRD) and Raman spectroscopy to investigate the impact of pre-annealing on the structural properties of the precursors and final CZTS films. Glow discharge optical emission spectroscopy (GDOES) shows that pre-annealing of the precursors can improve depth homogeneity of the CZTS films. Photoluminescence spectra and the optical band gap energy values are compatible with literature. Selected samples were processed to solar cells and characterized.

1. Introduction

Thin film solar cells are promising candidates for sustainable and inexpensive energy conversion in the future. Three thin film materials so far have been brought into commercial production of solar cells: thin film Si, Cu(In,Ga)Se_2 (CIGS), and CdTe [1,2]. Rare elements such as In and Ga may restrict the further development of CIGS based solar cell, despite the achievement of >21% conversion efficiency [3]. Also, the toxicity of Cd and limited supply of Te constrain the usage of CdTe-based solar cells.

Cu_2ZnSnS_4 (CZTS) has been studied as an alternative photovoltaic material, sharing a similar crystal structure with CIGS and containing abundant, environmentally friendly raw materials. The most stable structure of CZTS is kesterite which has a direct band gap of about 1.5 eV and a high absorption coefficient of over 10^4 cm^{-1} in the visible spectrum range [4]. Many different methods were developed for the growth of CZTS absorber layers. The fabrication processes can be classified in two parts: deposition of metallic precursors followed by annealing in a sulfur atmosphere. In the first part, deposition methods can be categorized as vacuum and non-vacuum techniques. Vacuum methods are for example pulsed laser deposition [5], thermal evaporation [6,7], e-beam evaporation [8], and magnetron sputtering [9–12]. The most commonly used non-vacuum methods are electrodeposition [13–15], spray pyrolysis [16,17], sol-gel deposition [18], doctor-blading or spin-coating of nanoparticles [19,20], or spin-coating or spray-deposition of molecular precursors [21]. In the second part of the fabrication, the annealing process can be performed using conventional thermal processing or using a rapid thermal processing (RTP) system, the latter allowing faster temperature ramping rates. This procedure can be performed using elemental sulfur vapor or an H_2S gas atmosphere. The maximum sulfurization temperature generally varies from 500 °C to 600 °C. The champion conversion efficiencies of around 8.4% for pure sulfide kesterite Cu_2ZnSnS_4 was achieved by Shin et al. [7] at first and later of around 9.6% by Kato et al. [22], which is still far from the theoretical Shockley-Queisser limit of about 32% for the conversion efficiency of CZTS thin film based solar cells [23]. It is difficult to find the best material growth parameters for absorber layers of high quality, in particular due to the possible formation of secondary phases [24]. High growth temperatures (>500 °C) are preferable for grain growth, however, these temperatures may lead to decomposition and loss of volatile elements and compounds such as metallic Zn and Sn-S. Unlike conventional thermal processing, RTP allows high ramp rates up to 50 K/s and shorter processing times, which may minimize decomposition reactions [25]. Also, rapid thermal processing is attractive for industrial fabrication due to its higher throughput and lower energy consumption.

* Corresponding author at: Helmholtz Zentrum Berlin Mat & Energie GmbH, D-14109 Berlin, Germany.
E-mail address: maliolgar@ktu.edu.tr (M.A. Olgar).

http://dx.doi.org/10.1016/j.tsf.2017.03.008
0040-6090/

Table 1
Prepared metallic films for CZTS.

Sample	Complete stacked films	Pre-annealing of Mo/Cu/Sn	Sulfurization temperature
I		–	
II	Mo/Cu/Sn/Zn/Cu	200 °C, 3 min	600 °C
III		380 °C, 6 min	

In this work it was tried to find a promising metallic precursor with and without a pre-annealing step of the Cu-Sn metallic layers, suitable for sulfurization with a RTP system. Using stacked Mo/Cu/Sn/Zn/Cu metallic films and RTP sulfurization at 600 °C for 3 min, we investigate and compare the impact of the pre-annealing treatment of Mo/Cu/Sn on the structural, optical and optoelectronic properties of the CZTS thin film absorber layers.

2. Experimental

Three types of stacked Mo/Cu/Sn/Zn/Cu films were fabricated using DC magnetron sputtering. The first type of film (I) was prepared by sequential deposition of the metallic precursor Mo/Cu/Sn/Zn/Cu. The thickness values targeted were in the range of 175, 230, and 165 nm for the Cu, Zn, and Sn layers, respectively. 70% of the Cu thickness was deposited on top of the Mo layer, and 30% on top of the Zn layer. The second type of film (II) was exposed to a pre-annealing treatment at 200 °C in vacuum after the deposition of Mo/Cu/Sn layers. The metal layer thicknesses were chosen in order to obtain a [Cu]/[Sn] ratio of 1.2 in the precursor film. The last type of film (III) was annealed at 380 °C in vacuum after deposition of the Mo/Cu/Sn layers ([Cu] / [Sn] = 1.2), to yield Cu-Sn alloys on Mo on which Zn and the final Cu was deposited afterwards. For comparing of the pre-annealing treatment and temperatures, these three kinds of films were prepared and denoted as I, II, and III type films (Table 1).

Metallic precursor layers were enclosed in a quartz box with a volume of approximately 200 cm^3. 300 mg sulfur was placed closed to samples and the quartz box was inserted in a RTP chamber. The quartz box was not vacuum tight but it provides sulfur vapor pressure up to 1 mbar. After achieving ~2×10^{-5} mbar base pressure in the RTP chamber the samples were heated by high radiation emitted by tungsten halogen lamps with a ramp rate of 5 °C/s up to a dwell temperature of 600 °C, which was kept for 3 min. The evaporated sulfur reacted with the hot metallic precursor layers. A thermocouple was attached close to the samples for temperature measurements. Cooling of the samples down to 60 °C were performed by turning of the lamps in vacuum before the RTP vented with nitrogen [26]. For removal of possible copper-sulfide phases segregated on the surface, samples were etched for 3 min in a 10% KCN solution. All of the absorber analyses were performed after KCN etching except for the first X-ray fluorescence (XRF) measurements. The compositional ratio of the films was checked by XRF before and after KCN etching to reveal whether copper-sulfide phases formed on the surface or not. The atomic ratio of the films was determined by XRF line scans (100 different points) with a step size of 50 μm. Generator settings were 300 μA and 30 kV and the exposure

Table 2
Atomic ratio of type I, II and III films before and after KCN etching. The precursor composition was estimated from weighing, whereas the processed absorbers (I–III) were measured by XRF.

Sample	Before KCN etching			After KCN etching		
	Cu/(Zn + Sn)	Cu/Sn	Zn/Sn	Cu/(Zn + Sn)	Cu/Sn	Zn/Sn
Precursor	0.77	1.75	1.26			
I	0.81	1.77	1.16	0.81	1.78	1.17
II	0.79	1.65	1.08	0.80	1.68	1.10
III	0.78	1.65	1.10	0.79	1.65	1.09

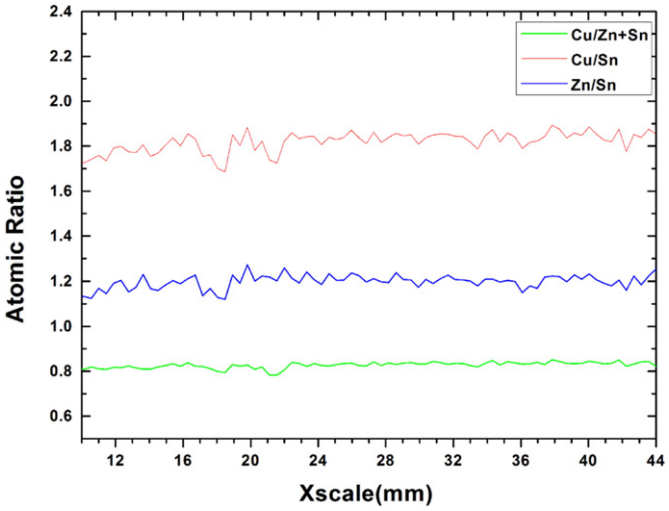

Fig. 1. Atomic ratio of the KCN etched type I kesterite film through the surface of the film.

time of each measurement was 60 s. The crystalline structure of the films was characterized by X-ray diffraction (XRD) using an X'pert Pro System with Bragg Brentano configuration (θ-2θ), using the CuK_α line ($\lambda = 1.54060$ Å) and with generator settings of 30 mA and 40 kV. Raman spectroscopy of the films were taken with a micro-Raman spectrometer (Dilor Labram Micro-Raman), where the wavelength of the excitation light was 633 nm, with a spot size of 3 μm and intensity of 2 W/cm^2. The surface and cross-section morphology of the films were characterized by a Gemini Leo 1530 scanning electron microscope (SEM). Depth profiles of the films were investigated by Glow Discharge Optical Emission Spectroscopy (GDOES, GDA650 Analyzer). The transmittance spectra of the films were obtained by a Dongwoo Optron spectrophotometer using 450 W Xe lamp in the spectral range of 600–1350 nm at room temperature. Optical band gap measurements were achieved by transferring the CZTS thin film layers from Mo-coated glass to pure cleaned glass by a peel-off technique. A similar procedure had been previously used for CIGS materials [27]. Photoluminescence measurements were performed at room temperature using an excitation laser at 670 nm and a 1/4 m spectrograph coupled to an InGaAs diode array. For solar cell applications, chemical bath deposition of a CdS buffer layer was obtained from cadmium acetate/ammonia solution added to thiourea solution at 60 °C for 7 min.

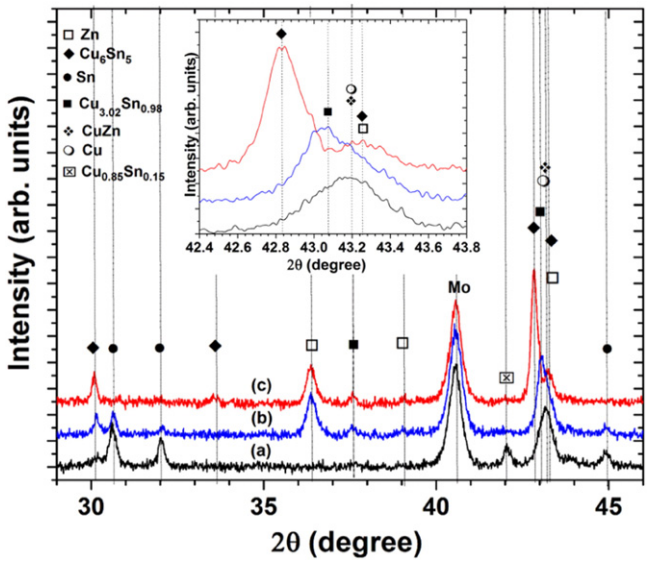

Fig. 2. X-ray diffraction pattern of a) I, b) II, and c) III type metallic precursor films.

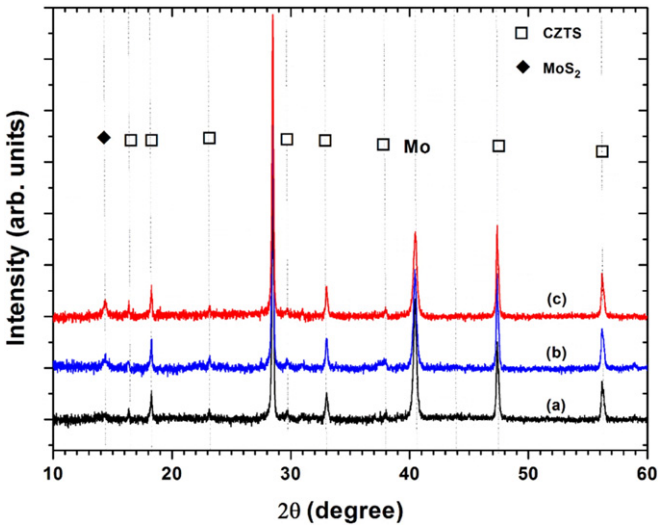

Fig. 3. X-ray diffraction pattern a) I, b) II, and c) III type of CZTS thin films.

The resulting CdS layer thickness is in the order of 40 nm. The window layer consisting of an i-ZnO/n^+-ZnO:Al double layer is deposited by RF sputtering. 130 nm i-ZnO are sputtered at 8 μbar with argon by addition of approximatively 1% of oxygen, followed by 240 nm of n^+-ZnO:Al layer sputtered at 1.5 μbar with pure argon. Solar cells were completed by evaporation of a metallic grid consisting of 20 nm nickel, 2 μm aluminium and another 20 nm of nickel. The device performance of the cells was characterized by current-voltage (I-V) measurements under AM 1.5 irradiation using a Steuernagel solar simulator. Its AM 1.5 spectrum was approximated by an Osram metal halogen lamp HMI 575 SE. Intensity calibration to 100 mW/cm^2 had been performed using a calibrated $CuInS_2$ solar cell with similar bandgap and a GaAs solar cell.

3. Results and discussion

All of the metallic precursor films were prepared Cu-poor and Zn-rich ([Cu] / [Zn + Sn] = 0.77, [Cu] / [Sn] = 1.75, [Zn] / [Sn] = 1.26) as determined by XRF. Table 2 presents atomic ratios of the sulfurized CZTS films before and after the KCN etching process. While all sulfurized films are also Cu-poor and Zn-rich, it is apparent that the Type I sample, which has not seen any pre-anneal treatment has a decreased Sn content after sulfurization, when compared to the pre-annealed samples.

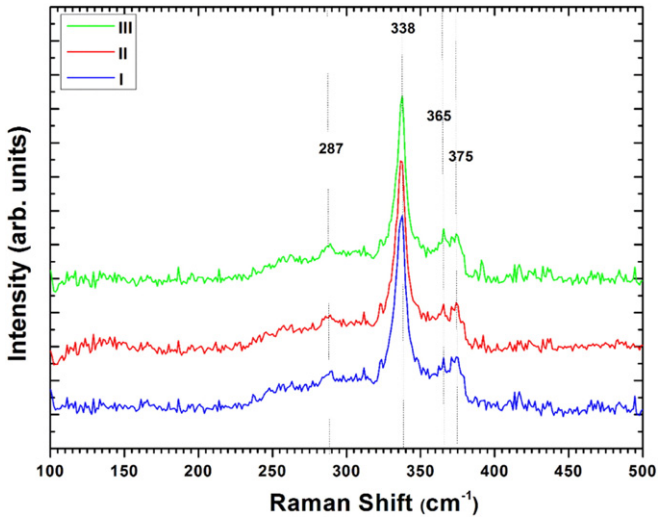

Fig. 4. Raman spectra of type I, II, and III type kesterite CZTS films.

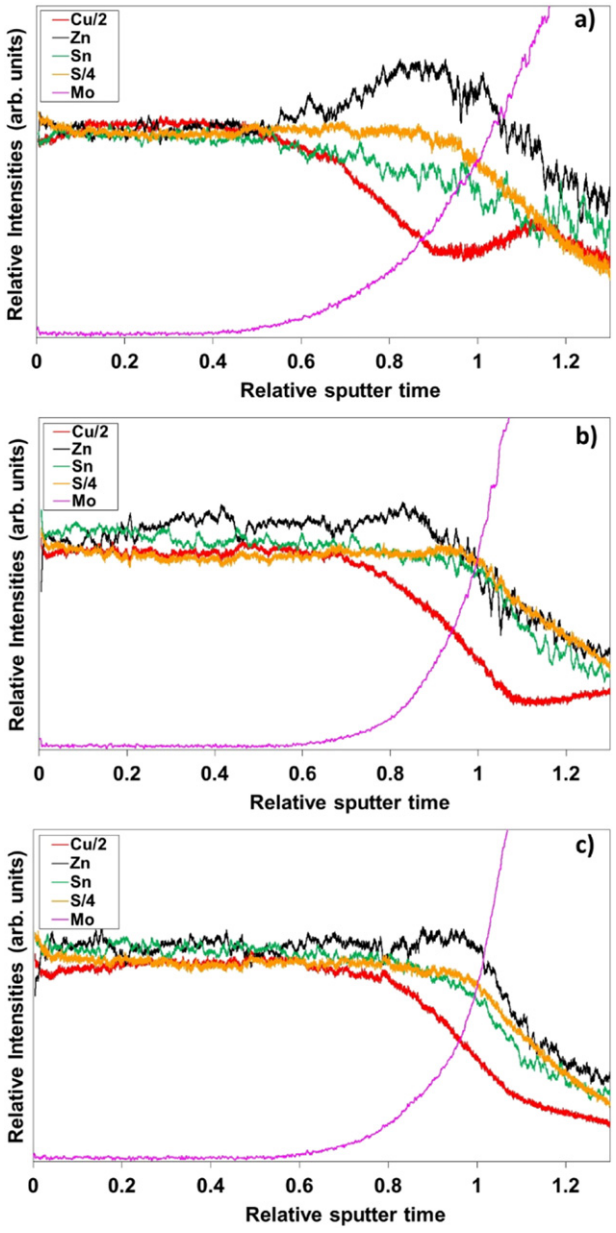

Fig. 5. Compositional depth profile of a) I, b) II, and c) III type kesterite CZTS films measured towards to back contact (left to right in the graph) by GDOES.

As can be seen from Table 2, the elemental compositional ratios of Cu/(Zn + Sn), Cu/Sn, and Zn/Sn have the same values before and after KCN etching for I, II, and III type kesterite films, when taking an experimental error of ±3 at% into account. Hence, there is no indication for the formation of copper sulfide phases at least in the top layers of the samples accessible to KCN etching.

XRF line scan measurements on the films show the lateral elemental distribution on the millimeter length scale. Fig. 1 displays variations of the elemental atomic ratios of the type I kesterite film after KCN etching. The fluctuation has a standard deviation of 0.04 for Cu/Sn and Zn/Sn, and 0.01 for Cu/Zn + Sn, and thus shows a relatively good macroscopic homogeneity of the films. Similar results have been found for the type II and type III films.

XRD patterns of the metallic precursor thin films of type I, II, and III are shown in Fig. 2(a–c). In the XRD pattern of the type I film (Fig. 2(a)) the alloy $Cu_{0.85}Sn_{0.15}$ [JCPDS 03-065-9056] (2θ = 42.03°) is observed in addition to the elemental peaks for Sn [JCPDS 01-086-2265] (2θ = 30.59°, 32°, 44.95°). Due to an overlap with Cu [JCPDS

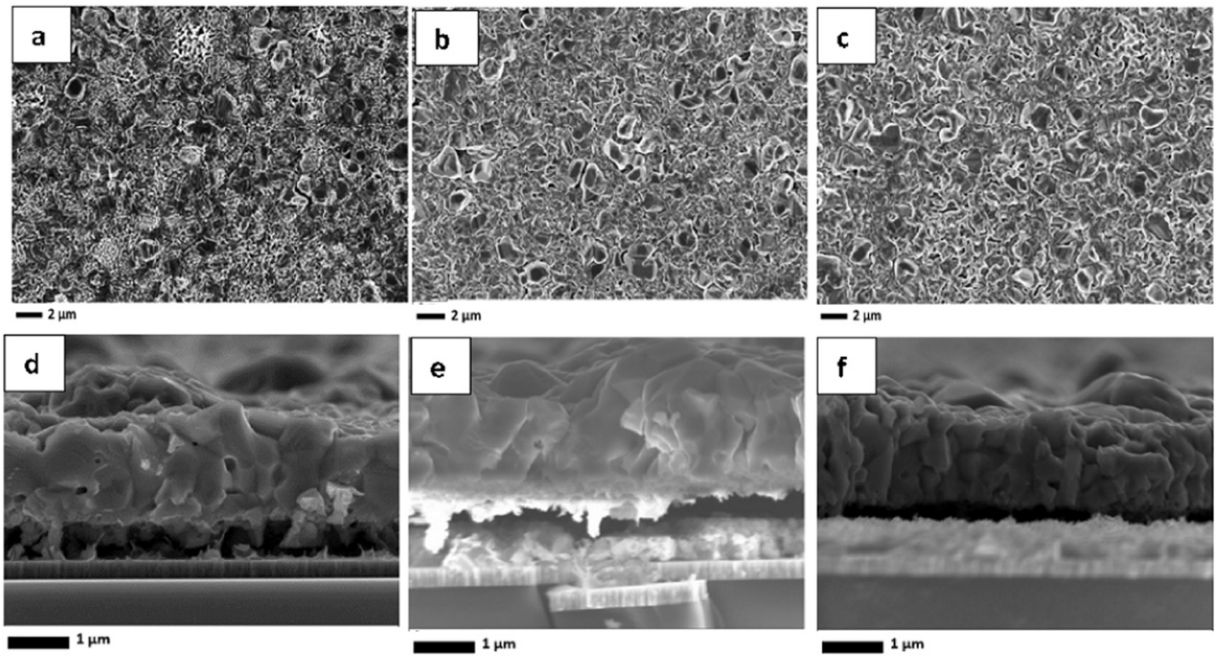

Fig. 6. SEM surface and cross-section microstructures of I (a, d), II (b, e), and III (c, f) type kesterite CZTS thin films.

01–070-3038] ($2\theta = 43.20°$), CuZn [JCPDS 03-065-9061] ($2\theta = 43.20°$) cannot be unambiguously identified. However since no elemental Zn or any other Zn alloy is observed, the contribution of CuZn to this peak is likely. In the XRD pattern of the type II precursor film (Fig. 2(b)) major changes are observed compared to the type I precursor film. It can be seen clearly that the elemental Sn phase is partly transformed to Cu-Sn alloy compounds such as Cu_6Sn_5 [JCPDS 05–2303] ($2\theta = 42.83°, 43.25°$) and Cu_3Sn [JCPDS 65–5721] ($2\theta = 43.07°$) as expected. Some elemental Sn is still observable, in addition to elemental Zn [JCPDS 04-0831] ($2\theta = 43.25°$). The $Cu_{0.85}Sn_{0.15}$ phase, which is metastable at room temperature, could not be detected in this film. This phase might have transformed into the more stable phase Cu_6Sn_5. For sample type III all metallic Sn is transformed to the Cu_6Sn_5 phase except for a residual minor peak of Cu_3Sn (Fig. 2(c)). In addition to the Cu-Sn alloy compounds, elemental Zn and Mo peaks also are observed in the structure. This indicates that the pre-annealing has mainly led to the formation of Cu-Sn alloys, as intended.

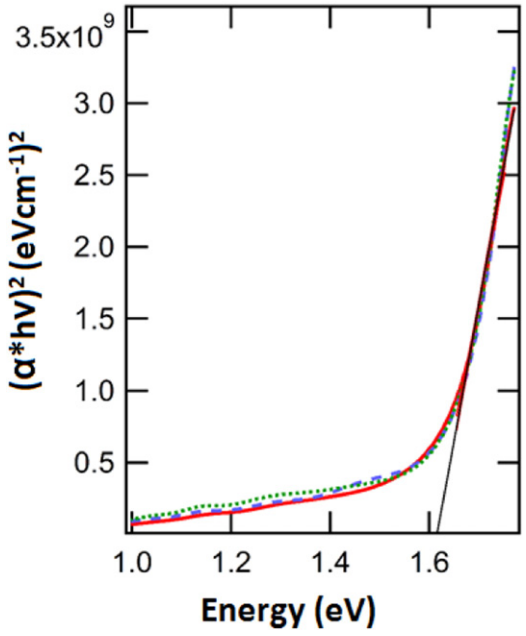

Fig. 7. Plot of $(\alpha h\nu)^2$ (eV $cm^{-1})^2$ versus photon energy ($h\nu$) (eV) for estimation optical band gap energy of I, II, and III type kesterite CZTS thin films.

Fig. 3 shows X-ray diffraction patterns of type I, II, III kesterite films after annealing in sulfur atmosphere at 600 °C. The XRD patterns for all three CZTS thin films shows dominant peaks at 28.5°, 33°, 47.33°, 56.17°, and 58.97°, which can be all assigned to either kesterite [JCPDS 26-0575], ZnS [JCPDS 05-0566] or Cu_2SnS_3 [JCPDS 027-0198]. However, weak superstructure peaks of kesterite are visible below 20° indicating the formation of kesterite, even if the presence of ZnS and Cu_2SnS_3 cannot be ruled out. The Mo 110 diffraction peak is observed at $2\theta = 40.51°$ in all films coming from the back contact [JCPDS 04–0809]. The XRD patterns for the differently processed samples are very similar, with the exception of the formation of MoS_2 [JCPDS 74-0932] at $2\theta = 14.30°$, which is only observed for films of type II and III.

In order to confirm the existence of the kesterite CZTS structure and to detect possible secondary phases indistinguishable from CZTS in XRD, Raman spectroscopy was performed [28]. Fig. 4 presents Raman spectra of the type I, II, and III CZTS kesterite films. In accordance with the XRD results, all of the films irrespective of the pre-annealing process of the Cu-Sn layer show similar Raman spectra. A strong major peak at 338 cm^{-1}, which is attributed to the preferential vibrational A mode of the kesterite CZTS phase is observed [29]. Other respectively minor but characteristic peaks of CZTS appear at around 287, 365, and 375 cm^{-1}. Although we have not observed a ZnS transition in our Raman measurements we cannot exclude presence of this secondary phase, because of the low Raman cross-section of the red laser light for ZnS [30].

Compositional depth profiles of the films were obtained using the GDOES technique. Fig. 5(a–c) shows compositional depth profiles of type I, II, and III kesterite films, respectively. The graphs present the elemental distribution in the films from the top surface to the molybdenum back contact. The intensities were normalized such that the plotted lines coincide for the case of perfect Cu_2ZnSnS_4 stoichiometry. Up to the points where the Mo signal starts to rise, all three films show nearly coinciding intensities of the four elements, indicating low concentrations of secondary phases in the main parts of the films.

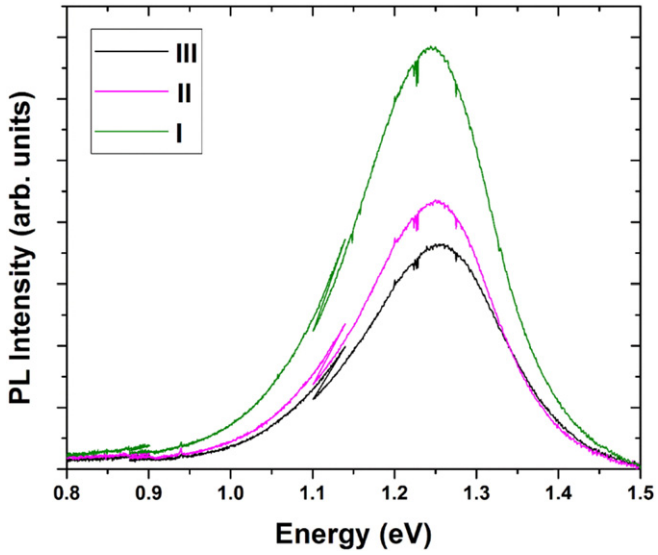

Fig. 8. PL spectrum of kesterite CZTS thin films at room temperature.

Near the back side of the films where they overlap with the Mo signal, the Cu, Zn, Sn and S signals deviate from each other, with a reduced Cu concentration in all three films. This indicates that secondary phases mainly form at the bottom of the films. The type I film shows the highest Zn intensity relative to Cu and Sn, which can be explained by a significant formation of ZnS at the bottom of the film. No clear evidence for MoS_2 formation can be derived from the GDOES data. However, since Mo_2S was observed for the type II and III films by XRD, we assume that the presence of MoS_2 contributes to some extend to the deviation of the concentrations from the CTZS stoichiometry near the back contact. The shallow slope of the Mo signal indicates that this film has a higher roughness or porosity than the type II and III films. The type II and III films do not show a significant difference. From these observations we conclude that the Mo/Cu/Sn/Zn/Cu precursor stack is suitable for the synthesis of films with fairly homogeneous element distributions in the bulk region of the films. The pre-annealing treatment of the Mo/Cu/Sn stack (II, III) seems to help to form smoother films and reduce the formation of ZnS at the back of the film.

SEM images of the type I, II, and III kesterite CZTS thin films are shown in Fig. 6(a–c). All of the films show a similar polycrystalline morphology. Fig. 6(d–f) exhibits micrographs of cross-sections taken for the I, II, and III type kesterite films, which also indicate a similar morphology, although the cross-section for the film obtained from the precursor annealed at 380 °C (type III) seems to indicate a somewhat more compact layer. From the similarity of the images we deduce that the different pre-annealing treatments do not have a major influence on the microstructure. We attribute the small, bright grains visible on the top surfaces to ZnS secondary phases [31,32].

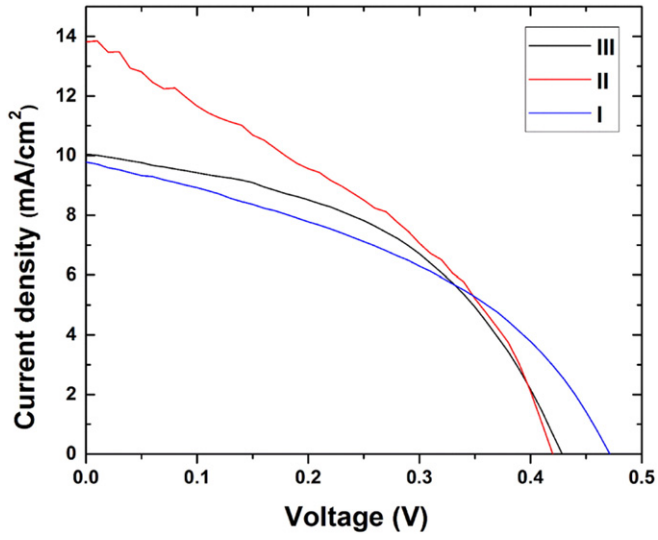

Fig. 9. *J-V* characteristic of the I, II, and III type kesterite-based solar cells.

Transmittance spectra of the CZTS thin films were measured to determine the band gap of the films. For this the absorption coefficient, α, was calculated using the Lambert-Beer law;

$$\alpha = \frac{1}{d}\ln\left(\frac{1}{T}\right) \quad (1)$$

where d is the thickness and T is the transmittance of the film. The band gap energy, E_g, is obtained from plotting $(\alpha h\nu)^2$ versus photon energy $(h\nu)$, and evaluating the intercept on the horizontal photon energy axis [33], as appropriate for direct band gap semiconductors. As shown in Fig. 7, the band gap values determined from the graph for all films are between 1.61 and 1.63 eV. The fact that the plotted quantity does not drop to zero in the subgap region can be explained with substantial band tailing extending into the gap, or parasitic absorption, e.g. due to Cu_2SnS_3 secondary phases. The reported band gap energy in the literature for kesterite CZTS thin film is 1.4–1.6 eV [34], with the band gap in high quality material most commonly reported at about 1.5 eV [35], which means that although the band gaps observed in this study are in agreement with the higher values reported in literature.

In Fig. 8 room temperature photoluminescence (PL) spectra of the kesterite films are shown. All PL emissions exhibit one broad asymmetric band which is peaked between 1.2 and 1.3 eV, which is considerably lower than the band gap energy value determined above. Similar asymmetric broad band values which are between 1.2 and 1.3 eV were previously reported [36–39] and have been attributed to conduction band to acceptor transitions and related recombination paths in CZTS thin films [37,39]. The fact that band-band transitions are not observed at room temperature indicates a very large concentration of deep acceptor levels in this material.

Fig. 9 shows the illuminated *J-V* characteristics of the corresponding solar cells of type I, II, III kesterite CZTS thin films. All of the solar devices show roughly a similar *J-V* behavior with small differences with respect to their photovoltaic parameters (Table 3). The type I, II, and III CZTS solar cells show open-circuit voltages of 471, 420, 428 mV, short-circuit currents of 9.8, 13.8, 10.3 mA/cm^2, fill factors of 0.41, 0.37, 0.47, and conversion efficiencies of 1.9, 2.2, 2.0% respectively.

All devices suffer from low open-circuit voltages as well as low short circuit currents, which indicates that the minority carrier lifetimes and diffusion lengths are rather low, due to excessive recombination. The short-circuit current density of the films may also be limited by the significant formation of ZnS at the back contact, as discussed above. The differences in the *JV* parameters for the 3 types of devices are not considered significant with respect to their preparation conditions.

4. Conclusion

In this study CZTS thin films were grown by DC magnetron sputtering for sequential metallic film deposition and sulfurization of the metallic films in sulfur vapor atmosphere using rapid thermal processing (RTP). To enhance the homogeneity of the films, pre-

Table 3
Photovoltaic parameters of I, II, and III type solar cells.

Sample	V_{oc} (mV)	J_{sc} (mA/cm^2)	η (%)	FF	R_s (Ω∗cm^2)
I	471	9.8	1.9	0.41	1.33
II	420	13.8	2.2	0.37	0.62
III	428	10.1	2.0	0.47	2.48

annealing treatments were applied at different temperatures after deposition of Cu and Sn on Mo coated glass, in order to preferentially alloy the Cu with Sn. From XRD analysis it is found that for a pre-annealing temperature of 380 °C most Sn is contained in Cu_6Sn_5, while most of the Zn is still in elemental form. XRD analysis of the sulfurized CZTS films shows specific kesterite superstructure peaks for all three precursor types, while the presence of ZnS and Cu_2SnS_3 cannot be ruled out. Formation of the CZTS crystal structure was confirmed using Raman spectroscopy. Depth profile analyses by GDOES showed that the pre-annealing process improved the compositional depth distribution of the films. The PL and optical band gaps of the films do not show significant differences with respect to optical properties due to pre-annealing process. The observed room temperature PL transition (~1.25 eV) and band gap energy (~1.61 eV) values are compatible with the literature, although the latter energy is rather large. The best solar cell had a V_{oc} of 420 mV, a J_s of 13.81 mA/cm^2, and an efficiency of 2.2%.

Acknowledgement

M.A. Olgar is grateful to Turkish Council of Higher Education (YÖK) for financial support in visiting foreign institution. We gratefully acknowledge the help of L. Steinkopf, C. Ferber and M. Kirsch with sample preparation, S. Levcenco and S. Kretzschmar for Raman measurements, A. Scheu for GDOES measurements, D.R. Wargulski for SEM measurements, and M. Tomakin for optical measurements. We also acknowledge the discussion in the whole Kesterite-team, especially J. Just.

References

[1] T. Unold, H.-W. Schock, Nonconventional (non-silicon-based) photovoltaic materials, Annu. Rev. Mater. Res. 41 (2011) 297–321.
[2] S. Delbos, Kësterite thin films for photovoltaics: a review, EPJ Photovolt. 3 (2012) 35004.
[3] P. Jackson, D. Hariskos, R. Wuerz, O. Kiowski, A. Bauer, T.M. Friedlmeier, M. Powalla, Properties of Cu(In, Ga)Se_2 solar cells with new record efficiencies up to 21.7%, Phys. Status Solidi (RRL) 9 (2015) 28–31.
[4] S.C. Riha, B.A. Parkinson, A.L. Prieto, Solution-based synthesis and characterization of Cu_2ZnSnS_4 nanocrystals, J. Am. Chem. Soc. 131 (2009) (12054-+).
[5] A.V. Moholkar, S.S. Shinde, A.R. Babar, K.U. Sim, Y.B. Kwon, K.Y. Rajpure, P.S. Patil, C.H. Bhosale, J.H. Kim, Development of CZTS thin films solar cells by pulsed laser deposition: Influence of pulse repetition rate, Sol. Energy 85 (2011) 1354–1363.
[6] C.W. Shi, G.Y. Shi, Z. Chen, P.F. Yang, M. Yao, Deposition of Cu_2ZnSnS_4 thin films by vacuum thermal evaporation from single quaternary compound source, Mater. Lett. 73 (2012) 89–91.
[7] B. Shin, O. Gunawan, Y. Zhu, N.A. Bojarczuk, S.J. Chey, S. Guha, Thin film solar cell with 8.4% power conversion efficiency using an earth-abundant Cu_2ZnSnS_4 absorber, Prog. Photovolt. 21 (2013) 72–76.
[8] H. Araki, A. Mikaduki, Y. Kubo, T. Sato, K. Jimbo, W.S. Maw, H. Katagiri, M. Yamazaki, K. Oishi, A. Takeuchi, Preparation of Cu_2ZnSnS_4 thin films by sulfurization of stacked metallic layers, Thin Solid Films 517 (2008) 1457–1460.
[9] S. Yazici, M.A. Olgar, F.G. Akca, A. Cantas, M. Kurt, G. Aygun, E. Tarhan, E. Yanmaz, L. Ozyuzer, Growth of Cu_2ZnSnS_4 absorber layer on flexible metallic substrates for thin film solar cell applications, Thin Solid Films 589 (2015) 563–573.
[10] M. Olgar, Y. Atasoy, B. Başol, M. Tomakin, G. Aygun, L. Ozyuzer, E. Bacaksız, Influence of copper composition and reaction temperature on the properties of CZTSe thin films, J. Alloys Compd. 682 (2016) 610–617.
[11] S. Marchionna, P. Garattini, A. Le Donne, M. Acciarri, S. Tombolato, S. Binetti, Cu_2ZnSnS_4 solar cells grown by sulphurisation of sputtered metal precursors, Thin Solid Films 542 (2013) 114–118.
[12] H. Katagiri, K. Jimbo, W.S. Maw, K. Oishi, M. Yamazaki, H. Araki, A. Takeuchi, Development of CZTS-based thin film solar cells, Thin Solid Films 517 (2009) 2455–2460.
[13] J.J. Scragg, P.J. Dale, L.M. Peter, Towards sustainable materials for solar energy conversion: Preparation and photoelectrochemical characterization of Cu_2ZnSnS_4, Electrochem. Commun. 10 (2008) 639–642.
[14] C.P. Chan, H. Lam, C. Surya, Preparation of Cu_2ZnSnS_4 films by electrodeposition using ionic liquids, Sol. Energy Mater. Sol. Cells 94 (2010) 207–211.
[15] M.I. Khalil, O. Atici, A. Lucotti, S. Binetti, A. Le Donne, L. Magagnin, CZTS absorber layer for thin film solar cells from electrodeposited metallic stacked precursors (Zn/Cu-Sn), Appl. Surf. Sci. 379 (2016) 91–97.
[16] N. Nakayama, K. Ito, Sprayed films of stannite Cu_2ZnSnS_4, Appl. Surf. Sci. 92 (1996) 171–175.
[17] M. Espindola-Rodriguez, M. Placidi, O. Vigil-Galan, V. Izquierdo-Roca, X. Fontane, A. Fairbrother, D. Sylla, E. Saucedo, A. Perez-Rodriguez, Compositional optimization of photovoltaic grade Cu_2ZnSnS_4 films grown by pneumatic spray pyrolysis, Thin Solid Films 535 (2013) 67–72.
[18] K. Tanaka, M. Oonuki, N. Moritake, H. Uchiki, Cu_2ZnSnS_4 thin film solar cells prepared by non-vacuum processing, Sol. Energy Mater. Sol. Cells 93 (2009) 583–587.
[19] C.J. Hages, S. Levcenco, C.K. Miskin, J.H. Alsmeier, D. Abou-Ras, R.G. Wilks, M. Bar, T. Unold, R. Agrawal, Improved performance of Ge-alloyed CZTGeSSe thin-film solar cells through control of elemental losses, Prog. Photovolt. 23 (2015) 376–384.
[20] G. Larramona, S. Levcenko, S. Bourdais, A. Jacob, C. Choné, B. Delatouche, C. Moisan, J. Just, T. Unold, G. Dennler, Fine-tuning the Sn content in CZTSSe thin films to achieve 10.8% solar cell efficiency from spray-deposited water–ethanol-based colloidal inks, Adv. Energy Mater. 5 (2015) 1501404.
[21] A. Collord, H. Xin, H. Hillhouse, Combinatorial exploration of the effects of intrinsic and extrinsic defects in CuZnSn(S,Se), IEEE J. Photovolt. 5 (2015) 288–298.
[22] T. Kato, H. Hiroi, N. Sakai, S. Muraoka, H. Sugimoto, Characterization of front and back interfaces on Cu_2ZnSnS_4 thin-film solar cells, Proceedings of the 27th European Photovoltaic Solar Energy Conference and Exhibition 2012, pp. 2236–2239.
[23] C.H. Henry, Limiting efficiencies of ideal single and multiple energy-gap terrestrial solar-cells, J. Appl. Phys. 51 (1980) 4494–4500.
[24] I.D. Olekseyuk, I.V. Dudchak, L.V. Piskach, Phase equilibria in the Cu_2S-ZnS-SnS_2 system, J. Alloys Compd. 368 (2004) 135–143.
[25] A. Fairbrother, L. Fourdrinier, X. Fontane, V. Izquierdo-Roca, M. Dimitrievska, A. Perez-Rodriguez, E. Saucedo, Precursor stack ordering effects in $Cu_2ZnSnSe_4$ thin films prepared by rapid thermal processing, J. Phys. Chem. C 118 (2014) 17291–17298.
[26] M.A. Olgar, J. Klaer, R. Mainz, S. Levcenco, J. Just, E. Bacaksiz, T. Unold, Effect of precursor stacking order and sulfurization temperature on compositional homogeneity of CZTS thin films, Thin Solid Films 615 (2016) 402–408.
[27] T. Umehara, S. Iinuma, A. Sadono, Y. Kurokawa, A. Yamada, Electrical characterization of Cu(In, Ga)Se_2 thin films peeled off from Mo-coated soda-lime glass substrate by AC Hall measurement, Jpn. J. Appl. Phys. 54 (2014) 018001.
[28] O. Vigil-Galan, M. Espindola-Rodriguez, M. Courel, X. Fontane, D. Sylla, V. Izquierdo-Roca, A. Fairbrother, E. Saucedo, A. Perez-Rodriguez, Secondary phases dependence on composition ratio in sprayed Cu_2ZnSnS_4 thin films and its impact on the high power conversion efficiency, Sol. Energy Mater. Sol. Cells 117 (2013) 246–250.
[29] H. Yoo, J. Kim, Comparative study of Cu_2ZnSnS_4 film growth, Sol. Energy Mater. Sol. Cells 95 (2011) 239–244.
[30] P. Fernandes, P. Salomé, A. Da Cunha, Study of polycrystalline Cu_2ZnSnS_4 films by Raman scattering, J. Alloys Compd. 509 (2011) 7600–7606.
[31] A. Weber, S. Schmidt, D. Abou-Ras, P. Schubert-Bischoff, I. Denks, R. Mainz, H.-W. Schock, Texture inheritance in thin-film growth of Cu_2ZnSnS_4, Appl. Phys. Lett. 95 (2009) 41904.
[32] C. Malerba, F. Biccari, C.L.A. Ricardo, M. Valentini, R. Chierchia, M. Müller, A. Santoni, E. Esposito, P. Mangiapane, P. Scardi, CZTS stoichiometry effects on the band gap energy, J. Alloys Compd. 582 (2014) 528–534.
[33] J. Pankove, Photoelectric Emission, Optical Processes in Semiconductors, 287, Dover Publications Inc., New York, 1971 301.
[34] N. Momose, M.T. Htay, T. Yudasaka, S. Igarashi, T. Seki, S. Iwano, Y. Hashimoto, K. Ito, Cu_2ZnSnS_4 thin film solar cells utilizing sulfurization of metallic precursor prepared by simultaneous sputtering of metal targets, Jpn. J. Appl. Phys. 50 (2011) (01BG09).
[35] B.A. Schubert, B. Marsen, S. Cinque, T. Unold, R. Klenk, S. Schorr, H.W. Schock, Cu_2ZnSnS_4 thin film solar cells by fast coevaporation, Prog. Photovolt. Res. Appl. 19 (2011) 93–96.
[36] Y. Miyamoto, K. Tanaka, M. Oonuki, N. Moritake, H. Uchiki, Optical properties of Cu_2ZnSnS_4 thin films prepared by sol-gel and sulfurization method, Jpn. J. Appl. Phys. 47 (2008) 596–597.
[37] S. Levcenko, V. Tezlevan, E. Arushanov, S. Schorr, T. Unold, Free-to-bound recombination in near stoichiometric Cu_2ZnSnS_4 single crystals, Phys. Rev. B 86 (2012) 045206.
[38] S. Levcenko, J. Just, A. Redinger, G. Larramona, S. Bourdais, G. Dennler, A. Jacob, T. Unold, Deep defects in $Cu_2ZnSn(S, Se)_4$ solar cells with varying Se content, Phys. Rev. Appl. 5 (2016) 024004.
[39] X. Lin, J. Kavalakkatt, K. Kornhuber, S. Levcenko, M.C. Lux-Steiner, A. Ennaoui, Structural and optical properties of Cu_2ZnSnS_4 thin film absorbers from ZnS and Cu_3 SnS_4 nanoparticle precursors, Thin Solid Films 535 (2013) 10–13.